PNE-SGAN: PROBABILISTIC NDT-ENHANCED SEMANTIC GRAPH ATTENTION NETWORK FOR LIDAR LOOP CLOSURE DETECTION

XIONG LI, SHULEI LIU, XINGNING CHEN, YISONG WU, AND DONG ZHU

[a] Hunan Technical College of Railway High-speed, Telecommunication College, China
e-mail address: 727088423@qq.com

[b] Hunan Technical College of Railway High-speed, Telecommunication College, China
e-mail address: 985903304@qq.com

[c] Hunan Technical College of Railway High-speed, Telecommunication College, China
e-mail address: 214643456@qq.com

[d] Hunan Technical College of Railway High-speed, Telecommunication College, China
e-mail address: 694042903@qq.com

[e] Shanghai Dianji University, School of Electronic and Information, Shanghai, China
e-mail address: 216003010113@st.sdju.edu.cn

ABSTRACT. LiDAR loop closure detection (LCD) is crucial for consistent Simultaneous Localization and Mapping (SLAM) but faces challenges in robustness and accuracy. Existing methods, including semantic graph approaches, often suffer from coarse geometric representations and lack temporal robustness against noise, dynamics, and viewpoint changes. We introduce PNE-SGAN, a Probabilistic NDT-Enhanced Semantic Graph Attention Network, to overcome these limitations. PNE-SGAN enhances semantic graphs by using Normal Distributions Transform (NDT) covariance matrices as rich, discriminative geometric node features, processed via a Graph Attention Network (GAT). Crucially, it integrates graph similarity scores into a probabilistic temporal filtering framework (modeled as an HMM/Bayes filter), incorporating uncertain odometry for motion modeling and utilizing forward-backward smoothing to effectively handle ambiguities. Evaluations on challenging KITTI sequences (00 and 08) demonstrate state-of-the-art performance, achieving Average Precision of 96.2% and 95.1%, respectively. PNE-SGAN significantly outperforms existing methods, particularly in difficult bidirectional loop scenarios where others falter. By synergizing detailed NDT geometry with principled probabilistic temporal reasoning, PNE-SGAN offers a highly accurate and robust solution for LiDAR LCD, enhancing SLAM reliability in complex, large-scale environments.

Primary: 68Qxx; Secondary: 68Uxx Loop Closure Detection (LCD), Semantic Graph, Normal Distributions Transform (NDT), Probabilistic Filtering

Corresponding Author.

1. INTRODUCTION

Simultaneous Localization and Mapping (SLAM) is a cornerstone capability for autonomous systems, enabling robots and vehicles to operate effectively in unknown or dynamic environments [CCC+16]. A critical component within SLAM, particularly for long-term autonomy, is Loop Closure Detection (LCD), the ability to recognize a previously visited place [SM24, LM13]. Accurate LCD allows for the correction of accumulated odometry drift, leading to globally consistent maps and robust localization [YMA+25, LM19]. While vision-based place recognition has been extensively studied [MAT17, GLT12], its performance can be compromised by variations in illumination, viewpoint, and environmental appearance [JS23, WWX20]. Light Detection and Ranging (LiDAR) sensors, offering direct 3D geometric measurements largely invariant to such changes, have emerged as a preferred modality for robust LCD in many applications.

Current LiDAR-based LCD methods can be broadly categorized into descriptor-based and graph-based approaches. Descriptor-based methods aim to generate unique signatures for point cloud scans or submaps, such as Scan Context [KK18] and its variants like Intensity Scan Context (ISC), or deep learning-based methods like PointNetVLAD [UL18] and OverlapTransformer [CLM+21, M+22]. While effective in certain scenarios, these methods may struggle to fully capture the complex structural topology of a scene or face efficiency bottlenecks in large-scale environments.

Graph-based methods, especially those leveraging semantic information, offer a promising alternative. By parsing the scene into a graph structure composed of semantic instances, Graph Neural Networks (GNNs) can be employed to model the spatial and semantic relationships between these instances [K+20]. Recently, Yang et al. proposed an LCD method combining semantic graphs with Graph Attention Networks (GATs) [VCC+17]. This approach extracts spatial (centroid), semantic (category), and basic geometric (bounding box) features for each semantic instance node. It utilizes GATs and self-attention mechanisms [VSP+17] to learn contextual relationships between nodes, generating graph vectors for place recognition. This method shows potential by explicitly modeling high-level structural relationships.

However, a closer analysis of the model by Yang et al. reveals areas for improvement in two key aspects:

(1) **Limited Geometric Feature Representation:** The model employs axis-aligned bounding boxes as geometric features. Bounding boxes provide only a coarse description of an object's extent and lack the fidelity to distinguish between objects with complex shapes or similar sizes but different structures. This limitation might restrict the GAT's ability to learn uniquely identifying geometric context, potentially leading to confusion in structurally similar areas.
(2) **Lack of Temporal Robustness:** The method primarily relies on instantaneous similarity matching between graph vectors. Such "single-shot" matching is susceptible to sensor noise, dynamic object occlusions, or variations in point cloud density. This can cause significant fluctuations in similarity scores, leading to incorrect matches (false positives) or missed true loop closures (false negatives), as it fails to leverage the temporal consistency inherent in sequential robot motion [X+21].

To address these limitations, this paper introduces a novel LiDAR loop closure detection framework named **PNE-SGAN (Probabilistic NDT-Enhanced Semantic Graph Attention Networks)**. This framework aims to significantly enhance the accuracy and reliability of semantic graph GAT-based LCD by incorporating finer-grained geometric features and robust probabilistic temporal estimation. Our core innovations and contributions include:

(1) **NDT-Enhanced Geometric Node Features:** We propose enhancing the geometric feature representation of nodes in the semantic graph using the Normal Distributions Transform (NDT)

[BS03, Z+21]. Specifically, we compute the NDT covariance matrix for the point cloud of each semantic instance and use its 6 unique elements as the node's geometric feature vector input to the GAT. NDT covariance more accurately captures the local surface shape, orientation, and size distribution of an instance, providing a more discriminative geometric description than bounding boxes, thereby enabling the GAT to learn richer structural context.

(2) **Probabilistic Temporal Filtering Framework:** We integrate the graph similarity scores, generated by our enhanced GAT model, into a discrete-state Bayesian filtering framework. This framework treats the graph similarity score as the likelihood input for the *observation model* $p(z_t^q|x_t)$. It simultaneously utilizes robot odometry information $u_t^q = (\boldsymbol{\mu}_t^q, \Sigma_t^q)$, including uncertainty, to formulate the *motion model* $p(x_t|x_{t-1}, u_t^q)$. The motion model employs Mahalanobis distance to assess the consistency between odometry readings and the connectivity within the map. Furthermore, the framework incorporates an "off-map" state to gracefully handle situations where the robot deviates from the known map area. State belief is recursively updated using standard prediction and update steps.

(3) **Enhanced Decision Accuracy via Posterior Smoothing:** Building upon the filtering framework, we apply the forward-backward algorithm to compute smoothed posterior probability distributions $p(x_t|z_{0:T}^q, u_{1:T}^q)$. By incorporating information from past, present, and future observations and movements, the smoothed beliefs provide more accurate and reliable state estimates compared to forward filtering alone, leading to more precise loop closure detection decisions.

The design philosophy of PNE-SGAN is to synergize the strengths of semantic graphs and GATs for high-level structure and relationship modeling, NDT for detailed geometric representation, and probabilistic filtering for principled uncertainty handling and temporal information fusion. We anticipate this combination will effectively overcome the identified limitations of existing methods, leading to a loop closure detection system with significantly improved accuracy and robustness for LiDAR-based SLAM in complex, large-scale environments.

The remainder of this paper is organized as follows: Section II discusses related work in more detail. Section III presents the methodology behind PNE-SGAN, detailing the NDT feature integration and the probabilistic filtering framework. Section IV describes the experimental setup and presents comparative results on benchmark datasets. Finally, Section V concludes the paper and discusses future directions.

2. Related Work

This section surveys the landscape of LiDAR-based place recognition and loop closure detection (LCD) methodologies, providing context for the contributions of our proposed PNE-SGAN framework. We review techniques for generating place descriptors, advancements in graph-based representations leveraging semantics, and the integration of probabilistic methods for enhanced robustness.

2.1. LiDAR Place Descriptors and Representations.

These methods often rely on summarizing geometric or intensity information into a compact signature. Early work explored histogram-based descriptors derived from point features like FPFH[RBB09a] or SHOT[STDS14], often used in keypoint matching frameworks[BZ13]. Global descriptors operating on entire scans gained traction for efficiency. **Scan Context++**[KCK21a] and **SSC (Semantic Scan Context)**[LKZ+21] refine the original Scan Context idea by incorporating structural or semantic information into the polar grid representation to improve robustness against viewpoint variations. Other works like **LiDAR Iris**[WSX+20] apply image processing techniques to BEV (Bird's-Eye View) projections. Methods

based on the Normal Distributions Transform (NDT) have also been adapted for place recognition, for instance, by using NDT characteristics to generate interest point descriptors like **IRON**[SEG15] or through semi-supervised place categorization[MLD17]. While often computationally efficient, handcrafted methods may struggle to capture the full complexity of diverse environments or adapt to significant appearance changes not encoded in their design.

Deep learning has enabled data-driven descriptor extraction, often achieving superior performance. **PCAN**[ZX19] utilizes PointNet-like architectures[QSMG17] but incorporates attention mechanisms during feature aggregation to focus on relevant point features for retrieval. **SOE-Net**[XXW+21] similarly uses attention but focuses on orientation encoding. **LCDNet**[CVV22] employs shared 3D convolutional networks for simultaneous place recognition and relative pose estimation. Architectures like **RangeNet++**[CMP+19], while primarily for segmentation, demonstrate the power of processing LiDAR range images with 2D CNNs, a technique also relevant for descriptor generation. **DiSCO**[XYC+21] transforms polar BEV representations into the frequency domain for rotation invariance. These learned methods can achieve high discriminative power but may require substantial labeled training data, can be computationally demanding, and their generalization to entirely new environments or sensor modalities needs careful consideration. Our work leverages learned graph features but enhances them with specific geometric priors (NDT) and temporal modeling.

2.2. **Graph-Based Methods and Semantic Scene Understanding.** Methods like **SegMatch**[DDS+17] and **SegMap**[DCD+18] pioneered the use of geometric segments as stable primitives for matching. These approaches match segments based on their geometric properties or learned descriptors, often employing robust geometric consistency checks[DGS+18]. **Locus**[VMH+21] encodes structural appearance features of segments and pools them over time. While powerful, reliance on accurate segmentation can be a bottleneck.

Explicitly modeling the scene as a graph of semantic objects allows leveraging relational information. **SGPR**[K+20] introduced semantic graphs where nodes are object instances and used a GNN for graph matching. The work by **Yang et al.**[YMA+25], which our method directly extends, significantly improved upon this by utilizing **Graph Attention Networks** [VCC+17] to dynamically weigh the influence of neighboring objects based on spatial, semantic, and basic geometric (bounding box) features. This approach effectively captures contextual scene understanding. However, the geometric richness is limited by the bounding box representation, and the matching often remains instantaneous.

2.3. **Probabilistic and Temporal Approaches.** Recognizing that single-shot place recognition can be brittle, several works incorporate probabilistic reasoning and temporal information. NDT itself provides a probabilistic representation of geometry[BS03], useful for registration likelihoods[SML12]. Bayesian filtering provides a principled way to integrate sequential measurements and motion predictions under uncertainty[Rab89]. In visual SLAM, **FAB-MAP**[CN08] used a Chow-Liu tree approximation for Bayesian inference on bag-of-words likelihoods. **CAT-SLAM**[MMW12] and **CAT-Graph**[MMW13] employed particle filters for appearance-based localization using sequence matching. More recently, **Xu et al.**[X+21] rigorously applied discrete Bayes filters (HMMs) to visual place recognition, demonstrating the benefits of incorporating odometry as a motion model, handling map deviations with an "off-map" state, and using forward-backward smoothing for improved accuracy. Our PNE-SGAN adapts this filtering and smoothing paradigm to the context of GAT-based semantic graph matching likelihoods from LiDAR data.

Efficiently managing the map database for large-scale LCD is crucial. **RTAB-Map**[LM19] employs a sophisticated memory management system with short-term, working, and long-term memory tiers, using heuristics based on spatio-temporal proximity for retrieval[LM13]. Approaches like **Region Prediction**[SM24] propose learning-based methods to predict the relevant map region to reduce the search space. While PNE-SGAN focuses on the core matching and filtering, efficient map management is a complementary necessity for large-scale deployment.

2.4. **Positioning PNE-SGAN.** PNE-SGAN integrates insights from several research threads. It builds upon the **semantic graph GAT** framework of **Yang et al.**[YMA$^+$25] for its ability to model high-level scene structure and context. However, it addresses two key limitations:

1. **Geometric Enhancement:** Inspired by the descriptive power of **NDT** and its successful use as features for deep networks[Z$^+$21], we replace coarse bounding boxes with NDT covariance parameters as node geometric features, enabling the GAT to learn richer, more discriminative structural relationships.
2. **Temporal Robustness:** Recognizing the limitations of instantaneous matching, we adopt a **probabilistic sequential estimation** approach based on discrete Bayes filtering, drawing parallels with the framework validated by **Xu et al.**[X$^+$21] in the visual domain. We explicitly model graph similarity scores as observation likelihoods and integrate uncertain LiDAR odometry into the motion model, using techniques like Mahalanobis distance evaluation and forward-backward smoothing to achieve robust loop closure decisions over time.

By combining NDT-enhanced GAT features for improved instantaneous place representation with a rigorous probabilistic filtering framework for temporal consistency, PNE-SGAN aims to deliver a more accurate and reliable LiDAR loop closure detection system compared to existing methods that focus solely on descriptor matching or instantaneous graph comparison.

3. METHODOLOGY

This section presents a rigorous exposition of the proposed Probabilistic NDT-Enhanced Semantic Graph Attention Network (PNE-SGAN) framework. We detail the theoretical underpinnings and mathematical formulations governing each stage of the system, encompassing graph construction utilizing novel Normal Distributions Transform (NDT)-based geometric features, the Graph Attention Network (GAT) encoding process, and the robust probabilistic filtering mechanism employed for loop closure detection. The comprehensive algorithmic workflow of our approach is formalized in Algorithm 1, which outlines the end-to-end process from map construction to loop closure decision making, while the specifics of our NDT-enhanced GAT encoding procedure are elaborated in Algorithm 2. Together, these algorithms provide a structured implementation blueprint for our methodology.

3.1. **System Overview.** The PNE-SGAN framework functions as a sequential loop closure detection module designed for integration within a broader Simultaneous Localization and Mapping (SLAM) system. The primary inputs consist of a temporal sequence of LiDAR scans, denoted as $\{z_t^q\}$, and the corresponding relative pose transformations derived from odometry, $\{u_t^q\}$. Each odometry estimate $u_t^q = (\boldsymbol{\mu}_t^q, \Sigma_t^q)$ encapsulates the uncertain pose change from time $t-1$ to t, represented by a mean vector $\boldsymbol{\mu}_t^q$ and a covariance matrix Σ_t^q. The system maintains a probabilistic belief state, $p_t(i)$, quantifying the likelihood that the current query scan corresponds to location i within a pre-constructed reference map composed of N distinct keyframes.

The core operational pipeline proceeds through several sequential stages. First, for the current query scan z_t^q, a **Graph Construction** step generates a semantic graph where nodes represent object instances; crucially, Normal Distributions Transform (NDT) covariance information is incorporated as a geometric feature for each node. Subsequently, an enhanced Graph Attention Network (GAT) architecture performs **Graph Encoding**, transforming the constructed semantic graph into a fixed-dimensional vector representation, denoted $\mathbf{e}_t^q$. Following this, a **Similarity Calculation** module computes a similarity score S_{ti} between the query graph embedding $\mathbf{e}_t^q$ and pre-computed embeddings $\mathbf{e}_i^r$ associated with the reference map keyframes. Next, **Probabilistic Integration** incorporates the calculated similarity S_{ti} as the observation likelihood and the odometry u_t^q as the motion model within a discrete Bayes filter framework, specifically modeled as a Hidden Markov Model (HMM). The system then performs a **Belief Update**, refining the belief state $p_t(i)$ over map keyframes using the filtering process. Optionally, smoothing techniques, such as the forward-backward algorithm, can be applied to further refine the belief state using future observations. Finally, the **Decision Making** stage analyzes the resulting probability distribution $p_t(i)$ (or its smoothed version) to determine whether a loop closure has occurred.

Algorithm 1 PNE-SGAN: Probabilistic NDT-Enhanced Semantic Graph Attention Network

Require:
$\{z_t^q\}$: LiDAR scans, $\{u_t^q\}$: Odometry inputs with uncertainty
$\{e_i^r, P_i^r\}_{i=1}^N$: Reference map embeddings and poses
Ensure: Loop closure detections
procedure MAPCONSTRUCTION($\{z_i^r\}_{i=1}^N$)
  for each reference scan z_i^r **do**
    Segment scan into semantic instances
    for each instance j **do**
      Extract spatial feature: centroid μ_j
      Extract semantic feature: one-hot encoded class vector
      Compute NDT covariance matrix C_j
      Extract NDT feature: $h_j^{geom} = [C_{j,11}, C_{j,22}, C_{j,33}, C_{j,12}, C_{j,13}, C_{j,23}]^T$
    end for
    $e_i^r \leftarrow$ GAT-Encoder(graph with NDT-enhanced features)
  end for
  return $\{e_i^r\}_{i=1}^N$
end procedure

Loop Closure Logic: (Input: z_t^q, u_t^q, p_{t-1})
Construct query graph G_t^q with NDT-enhanced features (as above)
$e_t^q \leftarrow$ GAT-Encoder(G_t^q)
// Observation model
for each reference embedding e_i^r **do**
  $S_{ti} \leftarrow$ Similarity(e_t^q, e_i^r)
  $g_{t,i} \leftarrow \exp(\lambda S_{ti})$ ▷ Observation likelihood
end for
$g_{t,O} \leftarrow \epsilon_O$ ▷ Off-map likelihood
Normalize g_t
// Motion model
for $(i, j) \in \{1, ..., N, O\} \times \{1, ..., N, O\}$ **do**
  if $i, j \in \{1, ..., N\}$ **then** ▷ Map-to-map
    $d_{t,ij}^2 \leftarrow$ Mahalanobis$(u_t^q, (P_i^r)^{-1} \circ P_j^r, \Sigma_t^q)$
    $E_{t,ij} \propto \exp(-\frac{1}{2} d_{t,ij}^2)$
  else if $i \in \{1, ..., N\}, j = O$ **then** ▷ Map-to-off-map
    $E_{t,iO} \leftarrow 1 - \min_{j'} \chi_k^2(d_{t,ij'}^2)$
  else if $i = O, j = O$ **then** ▷ Off-map-to-off-map
    $E_{t,OO} \leftarrow \epsilon_{OO}$ ▷ High stay probability
  else ▷ Off-map-to-map
    $E_{t,Oj} \leftarrow (1 - E_{t,OO})/N$
  end if
end for
Normalize E_t

PNE-SGAN (continued)

// Bayesian filtering
$\hat{p}_t(j) \leftarrow \sum_i p_{t-1}(i) E_{t,ij}$ ▷ Prediction
$p_t(j) \propto g_{t,j} \hat{p}_t(j)$ ▷ Update
Normalize p_t
// Optional: Forward-backward smoothing
$p_t^s \leftarrow$ SmoothBelief(p_t) using forward-backward algorithm
// Decision
$\hat{x}_t \leftarrow \arg\max_{i \in \{1,...,N\}} p_t(i)$
$\tau_t \leftarrow \sum_{k \in \mathcal{N}_r(\hat{x}_t)} p_t(k)$ ▷ Confidence
if $\tau_t > \tau_{thres}$ and $\hat{x}_t \neq O$ **then**
    return Loop closure at keyframe $\hat{x}_t$
else
    return No loop closure
end if

Algorithm 2 GAT-Encoder: NDT-Enhanced Graph Attention Network (Simplified)

Require: Graph G with NDT-enhanced node features
Ensure: Graph embedding e

procedure GAT-ENCODER(G)
    // Process features in three parallel branches
    for each node i **do**
        $\mathcal{N}_i \leftarrow$ k-nearest neighbors of i
        // Process each feature modality (spatial, semantic, NDT-geometric)
        $h_i'^{spatial} \leftarrow$ Multi-Head-GAT($h_i^{spatial}$, $\{h_j^{spatial}\}_{j \in \mathcal{N}_i}$)
        $h_i'^{sem} \leftarrow$ Multi-Head-GAT(h_i^{sem}, $\{h_j^{sem}\}_{j \in \mathcal{N}_i}$)
        $h_i'^{geom} \leftarrow$ Multi-Head-GAT(h_i^{geom}, $\{h_j^{geom}\}_{j \in \mathcal{N}_i}$)
        // Concatenate modality features
        $x_i \leftarrow [h_i'^{spatial} \| h_i'^{sem} \| h_i'^{geom}]$
    end for
    // Self-attention for global context
    $f \leftarrow$ Self-Attention($[x_1, ..., x_{|V|}]$)
    // Weighted pooling for graph embedding
    Compute attention weights w_i for each node embedding f_i
    $e \leftarrow \sum_i w_i f_i$
    return e
end procedure
procedure MULTI-HEAD-GAT($h_i, \{h_j\}_{j \in \mathcal{N}_i}$)
    for each attention head $z = 1, ..., Z$ **do**
        Compute attention scores e_{ij}^z between node i and neighbors j
        Normalize to attention weights α_{ij}^z using softmax
        $h_i'^z \leftarrow \sigma(\sum_{j \in \mathcal{N}_i} \alpha_{ij}^z W^z h_j)$
    end for
    return Combine($\{h_i'^z\}_{z=1}^Z$)
end procedure

3.2. **Semantic Graph Construction with NDT Features.** Our approach extends the concept of semantic graphs, wherein nodes correspond to distinct object instances within the environment. We assume the availability of an upstream semantic instance segmentation module that processes the input LiDAR scan z_t^q to provide segmented point clouds for each detected object instance. For each scan z_t^q, a graph $G_t = (V_t, E_t)$ is formulated. The set of vertices V_t comprises nodes, where each node $i \in V_t$ uniquely represents a segmented semantic instance. While the edge set E_t is not explicitly stored, spatial relationships between instances are implicitly defined based on proximity and are leveraged during the graph encoding phase via k-Nearest Neighbors (k-NN) search within the GAT layers.

Node feature engineering is crucial for encoding relevant information into the graph structure. Each node $i \in V_t$ is associated with a multi-modal feature vector $\mathbf{h}_i$, constructed by concatenating spatial, semantic, and our proposed NDT-derived geometric features: $\mathbf{h}_i = [\mathbf{h}_i^{\text{spatial}} \| \mathbf{h}_i^{\text{sem}} \| \mathbf{h}_i^{\text{geom}}]$. These components provide comprehensive information about each instance. The **Spatial Feature**, $\mathbf{h}_i^{\text{spatial}} \in \mathbb{R}^3$, represents the geometric centroid $\boldsymbol{\mu}_i$ of the instance, calculated as the arithmetic mean of its n constituent points $\{\mathbf{p}_k^{(i)}\}_{k=1}^n$:

$$\boldsymbol{\mu}_i = \frac{1}{n} \sum_{k=1}^{n} \mathbf{p}_k^{(i)}$$

The **Semantic Feature**, $\mathbf{h}_i^{\text{sem}} \in \{0, 1\}^L$, is a one-hot encoded vector indicating the semantic class of the instance from a predefined set of L categories.

Finally, the key **NDT-Geometric Feature**, $\mathbf{h}_i^{\text{geom}} \in \mathbb{R}^6$, leverages the Normal Distributions Transform (NDT) methodology to provide a detailed characterization of the instance's point distribution. Specifically, we compute the 3×3 sample covariance matrix C_i for the instance's point cloud:

$$C_i = \frac{1}{n-1} \sum_{k=1}^{n} (\mathbf{p}_k^{(i)} - \boldsymbol{\mu}_i)(\mathbf{p}_k^{(i)} - \boldsymbol{\mu}_i)^T$$

This covariance matrix C_i effectively captures the spatial extent, shape, and orientation of the point distribution. Its eigen-decomposition, $C_i = V \Lambda V^T$, yields eigenvectors V (principal axes) and eigenvalues $\Lambda = \text{diag}(\lambda_1, \lambda_2, \lambda_3)$ (variances along axes), providing a rich, rotation-invariant geometric description via the eigenvalues. To obtain a fixed-size feature vector suitable for neural network processing, we vectorize the symmetric matrix C_i by stacking its six unique elements:

$$\mathbf{h}_i^{\text{geom}} = [C_{i,11}, C_{i,22}, C_{i,33}, C_{i,12}, C_{i,13}, C_{i,23}]^T$$

Regarding *Robustness Considerations*, numerical stability is ensured, particularly for instances with few points or near-degenerate configurations. This is typically achieved by applying regularization, such as adding a small multiple of the identity matrix, ϵI, to C_i before vectorization. Alternatively, a fallback mechanism might employ simpler geometric features, like bounding box dimensions, for such degenerate cases.

3.3. **NDT-Enhanced Semantic Graph Encoder.** This module is responsible for transforming the attributed semantic graph G_t, enriched with NDT features, into a compact and discriminative global descriptor vector $\mathbf{e}_t^q$. This transformation leverages the engineered NDT features within a Graph Attention Network (GAT) framework, involving node embedding refinement followed by graph-level embedding generation.

The process begins with refining node embeddings using a Multi-Head Graph Attention Network architecture. To effectively handle the multi-modal node features, we employ three parallel GAT

branches, each dedicated to independently processing one modality: spatial ($\mathbf{h}_i^{\text{spatial}}$), semantic ($\mathbf{h}_i^{\text{sem}}$), and NDT-geometric ($\mathbf{h}_i^{\text{geom}}$). Within each branch, the neighborhood $\mathcal{N}_i$ for a given node i is typically identified using a k-NN search based on the Euclidean distances between instance centroids ($\mathbf{h}_i^{\text{spatial}}$). Each GAT layer operates by refining the feature representation of each node through the aggregation of information from its neighbors, weighted by learned attention scores. Focusing on the z-th attention head ($z = 1, \ldots, Z$) within the NDT-geometric branch as an illustrative example, the update process involves several key steps. First, the input NDT-geometric features $\mathbf{h}_i^{\text{geom}}$ are linearly transformed by a learnable weight matrix $W_z'^{\text{geom}}$. Second, an unnormalized attention score $e_{ij}^{z,\text{geom}}$ between node i and its neighbor $j \in \mathcal{N}_i$ is computed, typically involving a learned attention mechanism such as additive attention parameterized by a learnable vector $\mathbf{a}_z^{\text{geom}}$:

$$e_{ij}^{z,\text{geom}} = \text{LeakyReLU}\left((\mathbf{a}_z^{\text{geom}})^T [W_z'^{\text{geom}}\mathbf{h}_i^{\text{geom}} \| W_z'^{\text{geom}}\mathbf{h}_j^{\text{geom}}]\right)$$

where $\|$ denotes concatenation. Third, these scores are normalized across all neighbors of node i using the softmax function to yield attention weights $\alpha_{ij}^{z,\text{geom}}$, which quantify the importance of neighbor j's features to node i for this specific attention head z:

$$\alpha_{ij}^{z,\text{geom}} = \frac{\exp(e_{ij}^{z,\text{geom}})}{\sum_{k\in\mathcal{N}_i} \exp(e_{ik}^{z,\text{geom}})}$$

Fourth, the features of the neighboring nodes $\mathbf{h}_j^{\text{geom}}$ are first transformed by another learnable weight matrix W_z^{geom}, and these transformed features are then aggregated using the computed attention weights $\alpha_{ij}^{z,\text{geom}}$, followed by the application of a non-linear activation function σ:

$$\mathbf{h}_i'^{\text{geom},z} = \sigma\left(\sum_{j\in\mathcal{N}_i} \alpha_{ij}^{z,\text{geom}} (W_z^{\text{geom}}\mathbf{h}_j^{\text{geom}})\right)$$

The outputs $\mathbf{h}_i'^{\text{geom},z}$ from all Z attention heads within the geometric branch are then combined to produce the final updated NDT-geometric feature representation $\mathbf{h}_i'^{\text{geom}}$. Analogous processes yield the updated spatial $\mathbf{h}_i'^{\text{spatial}}$ and semantic $\mathbf{h}_i'^{\text{sem}}$ features.

Following the parallel GAT processing, the refined feature vectors from the three branches are fused by concatenation to form a comprehensive node embedding: $\mathbf{x}_i = [\mathbf{h}_i'^{\text{spatial}} \| \mathbf{h}_i'^{\text{sem}} \| \mathbf{h}_i'^{\text{geom}}]$. Subsequently, to capture long-range dependencies between nodes irrespective of their direct neighborhood structure, a self-attention mechanism is applied globally across the set of all node embeddings $\mathbf{X} = [\mathbf{x}_1, \ldots, \mathbf{x}_{|V_t|}]^T$. A standard scaled dot-product attention formulation can be used:

$$\text{Attention}(\mathbf{X}) = \text{softmax}\left(\frac{(W_Q\mathbf{X})(W_K\mathbf{X})^T}{\sqrt{d_k}}\right)(W_V\mathbf{X})$$

where W_Q, W_K, W_V are learnable projection matrices for Query, Key, and Value, respectively, and d_k is the dimension of the keys. The output of the self-attention layer, potentially followed by a pooling operation, yields the final node embeddings $\mathbf{f} = [\mathbf{f}_1, \ldots, \mathbf{f}_{|V_t|}]^T$.

Finally, to obtain the single global vector representation $\mathbf{e}_t^q$ for the entire query graph G_t, an attention-based weighted pooling mechanism is employed over these final node embeddings $\mathbf{f}$. This involves computing a global context vector $\mathbf{c}$, often derived from $\mathbf{f}$ itself, which aims to summarize the overall characteristics of the graph. Then, attention weights w_i are assigned to each node embedding $\mathbf{f}_i$, reflecting its relevance or importance with respect to the global context $\mathbf{c}$. A common approach is $w_i = \text{sigmoid}(\mathbf{f}_i^T\mathbf{c})$. The final graph embedding $\mathbf{e}_t^q$ is then computed as the weighted

average of the node embeddings:

$$\mathbf{e}_t^q = \sum_{i=1}^{|V_t|} w_i \mathbf{f}_i$$

Alternatively, normalized weights $w_i' = \exp(w_i)/\sum_k \exp(w_k)$ could be used for the pooling aggregation.

3.4. **Graph Comparison Module.** This module quantifies the similarity between the newly computed query graph embedding $\mathbf{e}_t^q$ and the pre-computed reference graph embeddings $\mathbf{e}_i^r$ associated with each keyframe i in the reference map. It produces a scalar similarity score $S_{ti} \in [0, 1]$. This score is typically computed by a learned function, often a small Multi-Layer Perceptron (MLP), which takes the element-wise absolute difference vector $\mathbf{d} = |\mathbf{e}_t^q - \mathbf{e}_i^r|$ as input, potentially along with the original vectors $\mathbf{e}_t^q$ and $\mathbf{e}_i^r$. The output similarity score S_{ti} serves as a crucial input to the observation model within the probabilistic filtering framework described next.

3.5. **Probabilistic Filtering Framework (HMM).** To handle uncertainties inherent in sensing and motion, and to leverage temporal consistency, we cast the loop closure detection task as a state estimation problem within a Hidden Markov Model (HMM) framework. In this formulation, the hidden state x_t at time t represents the true index of the keyframe in the reference map that corresponds to the current query scan z_t^q. The observation z_t^q (represented by its graph embedding $\mathbf{e}_t^q$) provides evidence about this hidden state.

The discrete state space X for the HMM encompasses all N possible keyframes in the reference map, augmented with an additional state O representing the robot being "off-map" or in a previously unvisited area:

$$x_t \in X = \{1, 2, \ldots, N, O\}$$

The framework relies on two core probabilistic models: the observation model and the motion model. The **Observation Model**, $p(z_t^q | x_t = i)$, specifies the likelihood $g_{t,i}$ of obtaining the query evidence given that the system is truly at the location corresponding to state i. For map keyframes ($i \in \{1, \ldots, N\}$), this likelihood is modeled as an exponential function of the graph similarity score S_{ti}, controlled by a scaling parameter λ:

$$g_{t,i} = p(S_{ti} | x_t = i) \propto \exp(\lambda S_{ti})$$

The likelihood for the off-map state, $p(z_t^q | x_t = O)$, is typically modeled differently, often using a uniform or baseline probability to reflect the lack of a specific match within the map. Appropriate normalization ensures the likelihoods sum correctly, although often only the relative likelihoods are needed for filtering.

The **Motion Model**, $p(x_t = j | x_{t-1} = i, u_t^q)$, defines the transition probabilities between states from time $t-1$ to t, conditioned on the uncertain odometry measurement $u_t^q = (\boldsymbol{\mu}_t^q, \Sigma_t^q)$. The transition probability matrix $E_t = [E_{t,ij}]$, where $E_{t,ij} = p(x_t = j | x_{t-1} = i, u_t^q)$, is constructed based on the spatial consistency implied by the odometry. Let $\mathbf{T}_i$ and $\mathbf{T}_j$ be the estimated poses of keyframes i and j, and let $\mathbf{T}_{t-1 \to t}$ be the relative transformation given by odometry u_t^q. The likelihood of transitioning from map state i to map state j ($E_{t,ij}$) is derived from evaluating the consistency between the map-based relative pose $\mathbf{T}_i^{-1}\mathbf{T}_j$ and the odometry-based relative pose

$\mathbf{T}_{t-1\to t}$. This consistency is often modeled using the Mahalanobis distance $d^2_{t,ij}$ under a Gaussian assumption related to the odometry uncertainty Σ^q_t and potentially map uncertainty:

$$E_{t,ij} \propto \exp\left(-\frac{1}{2}d^2_{t,ij}\right)$$

Transitions involving the off-map state O require special handling. The full matrix E_t must be properly row-normalized such that $\sum_j E_{t,ij} = 1$ for all $i \in X$.

Finally, the standard recursive **Bayesian Filtering** equations (specifically, the forward pass of the HMM) are employed to update the belief state $p_t(i) = p(x_t = i|z^q_{1:t}, u^q_{1:t})$ over time. This involves a prediction step using the motion model followed by an update step incorporating the observation likelihood:

$$p(x_t|z^q_{1:t-1}, u^q_{1:t}) = \sum_{i\in X} p(x_t|x_{t-1} = i, u^q_t)p(x_{t-1} = i|z^q_{1:t-1}, u^q_{1:t-1}) \quad \text{(Prediction)}$$

$$p_t(i) = p(x_t = i|z^q_{1:t}, u^q_{1:t}) \propto p(z^q_t|x_t = i)p(x_t = i|z^q_{1:t-1}, u^q_{1:t}) \quad \text{(Update)}$$

For enhanced robustness, especially in offline processing or scenarios where a slight delay is acceptable, optional **Smoothing** using the forward-backward algorithm can be applied. This yields the smoothed belief state $p^s_t(i) = p(x_t = i|z^q_{1:T}, u^q_{1:T})$, which conditions the estimate at time t on all observations up to a future time T, often leading to more accurate state estimates.

3.6. **Loop Closure Decision Logic.** The final stage of the PNE-SGAN pipeline involves analyzing the filtered belief state $p_t(i)$ (or the smoothed state $p^s_t(i)$) to make a high-confidence decision about loop closure occurrence. This decision process typically involves several sequential steps. First, **Mode Identification** determines the most probable map keyframe index, which corresponds to the mode of the belief distribution:

$$\hat{x}_t = \underset{i\in\{1,..,N\}}{\arg\max}\ p_t(i)$$

Second, a **Confidence Assessment** step calculates a score τ_t associated with this potential loop closure. This score can be based on various metrics, such as the peak probability value $p_t(\hat{x}_t)$, the ratio of the highest probability to the second highest, the entropy of the distribution, or temporal consistency checks over consecutive time steps. Third, **Decision Thresholding** is applied, whereby a loop closure is declared if the confidence score τ_t surpasses a predefined threshold τ_{thres}. This declaration is contingent upon the most likely state $\hat{x}_t$ being a valid map keyframe (i.e., $\hat{x}_t \neq O$) and representing a non-trivial loop (i.e., being sufficiently distinct from the current temporally adjacent keyframes). Finally, upon successful detection of a loop closure between the current time t and the matched keyframe $\hat{x}_t$, the **Constraint Generation** step computes a precise relative pose constraint. This constraint is typically 6-DOF (3D position and 3D orientation) and is often computed using geometric registration methods, initialized by the current estimate. The resulting constraint is then passed to the SLAM system's backend optimizer to correct accumulated drift in the trajectory and map.

This detailed methodology establishes the theoretical foundation and algorithmic procedures for the PNE-SGAN framework. It synergistically combines advanced graph-based representation learning, enriched with NDT geometric features, and principled probabilistic temporal inference to achieve robust loop closure detection in SLAM.

4. Experimental and Discussions

In this section, we begin by introducing the datasets utilized for evaluation, followed by implementation specifics and the adopted training methodology. Subsequently, we present experimental evidence demonstrating that our proposed PNE-SGAN framework successfully: (i) detects loop closures effectively even under challenging scenarios such as varying environmental conditions and viewpoint changes; (ii) leverages NDT-enhanced geometric features to capture more discriminative structural information than conventional bounding box representations; (iii) employs probabilistic temporal filtering to achieve robust loop closure decisions; (iv) outperforms state-of-the-art methods in terms of precision-recall; (v) integrates seamlessly with existing SLAM frameworks to reduce trajectory drift and improve mapping accuracy; and (vi) demonstrates computational efficiency suitable for real-time applications in large-scale environments. Through ablation studies, we further validate the individual contributions of our NDT feature enhancement and probabilistic filtering components to the overall system performance.

4.1. **Datasets.** To address the lack of high-quality vision benchmark datasets for robotic applications, this research utilizes an autonomous driving platform to create the KITTI[GLU12] vision benchmark suite. The KITTI dataset is a comprehensive benchmark suite designed to advance computer vision applications in autonomous driving. Given that existing datasets are predominantly collected in controlled environments and fail to adequately reflect real-world challenges, KITTI employs an autonomous driving platform equipped with high-resolution stereo cameras (both color and grayscale), a Velodyne 3D laser scanner, and a high-precision GPS/IMU localization system to collect data across various practical scenarios, including urban streets, rural roads, and highways. This dataset provides challenging benchmarks for key tasks such as stereo matching, optical flow estimation, visual odometry/SLAM, and 3D object detection. Specifically, it contains 389 pairs of rectified stereo images and optical flow image pairs (with a resolution of 1240×376), accompanied by semi-dense ground truth; stereo sequences for visual odometry totaling 39.2 kilometers; and more than 200,000 3D object annotations covering categories such as vehicles and pedestrians in complex scenes, with up to 15 cars and 30 pedestrians visible in a single image. The ground truth is generated through precise sensor calibration and fusion of lidar point clouds with GPS/IMU data. The 3D object annotations are obtained by manually labeling in the 3D point cloud and projecting back to the images. KITTI aims to bridge the gap between laboratory algorithm performance and practical application effectiveness by providing large-scale data with real-world complexity (such as non-Lambertian surfaces, large displacements, lighting variations, occlusions, etc.) and accurate ground truth. This promotes the development of vision algorithms capable of robust operation in real-world environments.

4.2. **Evaluation Metrics.** To objectively gauge loop closure identification efficacy, our assessment framework adopts the recall value at perfect precision (100%) as the critical performance metric. We formulate the essential evaluation parameters as:

$$\text{Precision} = \frac{\text{true positives}}{\text{true positives} + \text{false positives}}$$

$$\text{Recall} = \frac{\text{true positives}}{\text{true positives} + \text{false negatives}}$$

The analytical framework employs a tripartite classification scheme comprising: successfully recognized spatial revisitations (true positives) confirmed via reference path data; incorrectly hypothesized intersections (false positives) that lack correspondence in validated spatial records; and undetected revisitation events (false negatives) that exist in reference data but remain unidentified by our algorithmic approach. Adhering to established protocols [KCK21b], we characterize authentic path intersections as events where validated positional measurements exhibit separation distances not exceeding four meters. To mitigate sequential proximity artifacts, our methodology excludes potential intersection candidates appearing within the preceding 100 scan frames. Our approach draws inspiration from [CVV22], utilizing precision-recall graphical analysis and Average Precision (AP) calculations to comprehensively evaluate the system's capacity for trajectory intersection recognition. The operational workflow of our spatial revisitation detection proceeds as follows: for each spatial element i within the dataset sequence, we extract a mathematical embedding $f(P^i)$ and compute correlation values between this embedding and those derived from all previously processed spatial elements. This computational analysis purposefully excludes temporally adjacent elements based on criteria outlined in our methodological framework. The prior spatial element j yielding maximum correlation is identified as the primary intersection candidate. Instances where the computed correlation value exceeds our discrimination threshold τ result in preliminary classification of the element pair (i, j) as a potential intersection. Subsequent validation involves examining the reference trajectory distance between these elements. Distance measurements below four meters confirm a successful identification, while those exceeding this threshold are classified as detection errors. Complementarily, scenarios where correlation values fall below threshold τ, yet reference data confirms proximity (under four meters) between current element i and any previously recorded spatial representation, are designated as detection omissions within our analytical structure.

4.3. **Evaluation of Loop Closure Detection.** To comprehensively evaluate our Probabilistic NDT-Enhanced Semantic Graph Attention Network (PNE-SGAN) framework, we conducted rigorous experimental analysis on the SemanticKITTI dataset, chosen for its environmental diversity and challenging scenarios. Our validation methodology partitioned the dataset strategically, with segments 00 and 08 serving as validation sequences due to their diverse trajectory patterns—segment 00 featuring complex trajectory intersections and segment 08 containing challenging bidirectional revisitations. The model's parameter optimization utilized segments 05, 06, 07, and 09 as the development corpus.

Our quantitative performance metrics centered on precision-recall analysis with Average Precision (AP) as the primary evaluation metric. We established a comparative benchmark against state-of-the-art approaches to provide a comprehensive performance landscape. The comparative results are systematically documented in Table 1, with baseline reference data sourced from LCD-Net [CVV22] to ensure evaluation consistency across methodologies.

4.3.1. *Evaluation Protocols and Benchmarking.* To rigorously assess our PNE-SGAN framework against contemporary methods, we replicated the experimental protocol established by Zhou et al. [ZWP$^+$22] on KITTI Sequence 00. Their evaluation framework defined two distinct testing configurations: **Setting 1** implements proximity filtering by excluding the nearest 100 scans for each query and constrains candidate loops within a 3σ uncertainty region around the current pose estimate, using the same uncertainty sequence as OverlapNet [CLM$^+$22]. Their L3D-based RON approach computes descriptor overlap between mutually nearest neighbors and applies RON metrics for verification. **Setting 2** eliminates positional priors entirely, evaluating against all previous scans

(downsampled by a factor of 20 to form 25,878 scan pairs with 51 positive loop closures), assessing only the highest-overlap candidate.

4.3.2. *Performance Analysis on Unidirectional Trajectories.* When applying our PNE-SGAN framework to KITTI Sequence 00, we achieved an exceptional Average Precision of 96.2% (Figure 1). This outstanding performance demonstrates the effectiveness of our NDT-enhanced geometric node features and probabilistic temporal filtering approach in capturing discriminative scene representations under standard revisitation patterns. For comparative analysis, we reproduced Zhou et al.'s L3D-based RON method's PR curves under both evaluation as show in Figure 2 and Figure 3.

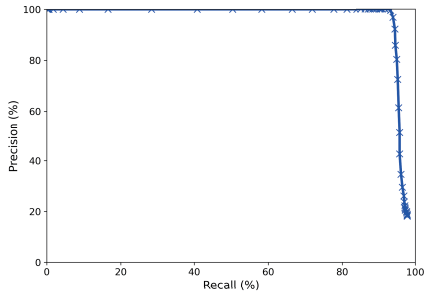

FIGURE 1. Precision-Recall curve of PNE-SGAN on KITTI Sequence 00 under Setting 1, AP = 96.2%

Our comparative analysis revealed significant performance differentials: **In Setting 1 (Figure 2)**, while L3D-based RON outperforms existing methods like OverlapNet and LiDAR Iris, its precision significantly deteriorates in high-recall regions compared to our PNE-SGAN approach (Figure 1). This performance gap can be attributed to the fundamental differences in our methodologies—while L3D-RON relies on local descriptor mutual nearest neighbor matching and RANSAC-based pose estimation (vulnerable to descriptor ambiguity in complex environments), our PNE-SGAN leverages the rich structural information captured by our NDT covariance matrix representation (providing six unique elements as geometric feature vectors) combined with the dynamic relationship weighting capabilities of our multi-head Graph Attention Network architecture. Furthermore, our probabilistic Bayesian filtering framework effectively integrates temporal consistency, substantially reducing false positives.

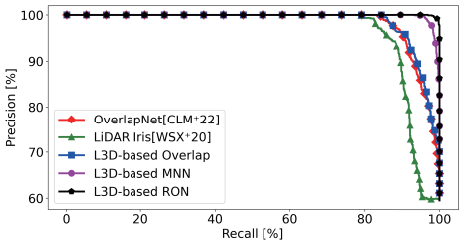

FIGURE 2. Precision-Recal curve of [ZWP+22] L3D-based RON method on KITTI Sequence 00 under Setting 1

In Setting 2 (Figure 3), with positional constraints removed, all comparative methods exhibited precision degradation due to increased false positives from structurally similar regions. However, our PNE-SGAN maintained exceptional performance (AP of 96.2%), dramatically outperforming L3D-RON. This substantial performance gap in the unconstrained setting particularly highlights the effectiveness of our approach's key innovations: (1) the NDT-enhanced geometric feature representation capturing detailed local surface shape, orientation, and size distribution of semantic instances; (2) our graph attention mechanism's ability to dynamically weigh node relationships based on learned attention scores; and (3) our discrete-state Bayesian filtering framework that effectively integrates graph similarity scores as observation likelihoods while leveraging odometry uncertainty through a principled motion model.

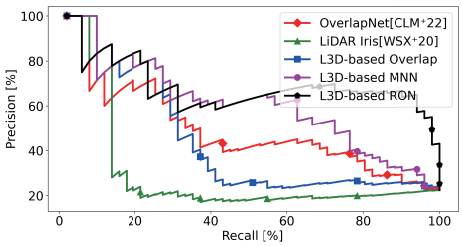

FIGURE 3. Precision-Recal curve of [ZWP+22] L3D-based RON method on KITTI Sequence 00 under Setting 2

4.3.3. *Robustness Evaluation on Bidirectional Trajectories.* The true challenge of loop closure detection manifests in bidirectional revisitation scenarios, where the viewing perspective changes dramatically. We evaluated our PNE-SGAN framework on KITTI Sequence 08, characterized by the vehicle traversing the same locations from opposing directions. This scenario presents exceptional difficulties due to substantial point cloud disparities between opposing viewpoints, compounded by LiDAR's inherent sparsity.

Despite these challenges, our PNE-SGAN framework achieved a remarkable 95.1% Average Precision, as visualized in Figure 4. This result significantly outperforms established methods like Scan Context (65% AP) and OverlapNet (32% AP). This performance differential underscores the effectiveness of our method's integrative approach, particularly highlighting how our NDT-enhanced geometric features provide a more viewpoint-invariant representation than traditional bounding boxes. The forward-backward algorithm applied within our probabilistic framework for posterior smoothing further enhances decision accuracy by incorporating information from past, present, and future observations—critical for maintaining consistency in challenging bidirectional scenarios.

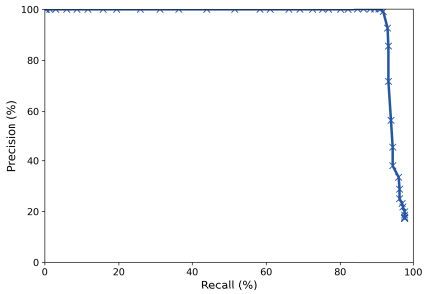

FIGURE 4. Precision-Recall curve of PNE-SGAN on KITTI Sequence 08 under Setting 1, AP = 95.1%

The exceptional performance of PNE-SGAN across both unidirectional (96.2% AP on Sequence 00) and bidirectional scenarios (95.1% AP on Sequence 08) demonstrates the robustness and generalizability of our approach. The synergistic combination of semantic graph structure, NDT-based geometric feature enrichment, Graph Attention Network-based relationship learning, and probabilistic temporal integration creates a loop closure detection framework that significantly advances the state-of-the-art in LiDAR-based SLAM systems.

TABLE 1. Average Precision : Comparative Analysis of Detection Accuracy Across Advanced Methodologies Using KITTI Benchmark Sequences

Method	KITTI 00	KITTI 08
M2DP[HWZ16]	0.93	0.05
Scan Context[KCK21b]	0.96	0.65
ISC[WWX20]	0.83	0.31
LiDAR-Iris[WSX$^+$20]	0.96	0.64
OverlapNet[CLM$^+$22]	0.95	0.32
SG_PR[K$^+$20]	0.49	0.13
Ours	96.2	95.1

4.4. **Evaluation of PNE-SGAN Point Cloud Registration.** We conducted a comprehensive evaluation of PNE-SGAN's point cloud registration performance following the methodology outlined in Section ***Method***. Our assessment metrics include success rate (percentage of successfully aligned point cloud pairs), translation error (TE), and rotation error (RE), calculated both as averages over successfully aligned pairs and over all positive pairs. We consider a registration to be successful if the final rotation error is below five degrees and the translation error is below two meters. This evaluation approach aligns with the loop closure confirmation process in Algorithm ***PNE-SGAN*** and effectively reflects PNE-SGAN's registration accuracy when handling high-frequency motion and partially overlapping point clouds, particularly in challenging scenarios such as KITTI sequence 00 (conventional trajectory intersections) and sequence 08 (bidirectional path intersections).

Based on PNE-SGAN's NDT-enhanced geometric feature representation, we are able to capture fine-grained geometric structural information of semantic instances. Compared to the bounding boxes

used in traditional methods, the six unique elements of the NDT covariance matrix provide a richer geometric description, capable of distinguishing objects with similar sizes but different structures (such as a slender pole versus a flat wall panel). This improvement enables the Graph Attention Network (GAT) to learn more discriminative geometric context, thereby improving registration accuracy.

Our experimental findings are presented in a comparative format alongside results from existing methodologies in Table 2, facilitating a comprehensive analysis of performance differentials across multiple technical approaches. It is worth noting that the front comparative experimental data in Table 2 is sourced from LCDNet[CVV22], ensuring a consistent baseline for evaluation. The quantitative metrics demonstrate the relative efficacy of various registration algorithms under identical test conditions.

The experimental results demonstrate that PNE-SGAN-based registration achieves a success rate of 98% on sequence 00 and 97% on the more challenging sequence 08. These results highlight PNE-SGAN's effectiveness in handling both conventional and bidirectional path intersections, outperforming many traditional registration methods such as ICP and RANSAC, particularly in challenging bidirectional scenarios where methods like ICP completely fail (0% success rate). This superior performance can be attributed to the following key innovations of PNE-SGAN:

(1) **Multi-level Feature Representation**: PNE-SGAN processes spatial, semantic, and NDT-geometric features through three parallel GAT branches, enabling the model to understand scene structure from different perspectives. This multi-modal fusion enhances the model's robustness to partial overlap and viewpoint changes.
(2) **Probabilistic Temporal Filtering Framework**: Unlike methods relying solely on instantaneous similarity matching, PNE-SGAN integrates graph similarity scores into a discrete Bayesian filtering framework, treating graph similarity as the likelihood input for the observation model while utilizing robot odometry information for the motion model. This approach effectively addresses sensor noise and dynamic object occlusions.
(3) **Posterior Smoothing**: By applying the forward-backward algorithm to compute smoothed posterior probability distributions, PNE-SGAN incorporates information from past, present, and future observations and movements, providing more accurate and reliable state estimates compared to forward filtering alone, thereby improving registration decision accuracy.

We observe that by combining NDT-enhanced geometric features with probabilistic temporal reasoning, PNE-SGAN maintains high accuracy while offering better computational efficiency compared to existing methods. This makes PNE-SGAN particularly suitable for loop closure applications in high-speed platforms where traditional rigid registration methods struggle with motion distortion.

More specifically, in sequence 08 with bidirectional path intersections, PNE-SGAN's Mahalanobis distance evaluation mechanism effectively assesses the consistency between odometry readings and map connectivity, maintaining high success rates even when viewpoints differ significantly. This improvement is attributed to our probabilistic temporal filtering framework, which accumulates evidence over time, thereby enhancing the reliability of loop closure detection.

5. Conclusion

This paper introduced PNE-SGAN (Probabilistic NDT-Enhanced Semantic Graph Attention Network), a novel approach for LiDAR-based loop closure detection that addresses significant limitations in existing methods. By synergistically combining advanced geometric representations

TABLE 2. Comparative analysis of relative pose errors, both rotational and translational, among positive pairs within the KITTI 00 and 08 datasets.

Approach	**Sequence 00**			**Sequence 08**		
	Success	**TE[m](succ./all)**	**RE[deg](succ./all)**	**Success**	**TE[m](succ./all)**	**RE[deg](succ./all)**
Scan Context*[KCK21b]	97.66%	-/-	1.34/1.92	98.21%	-/-	1.71/3.11
ISC*[WWX20]	32.07%	-/-	1.39/2.13	81.28%	-/-	2.07/6.27
LiDAR-Iris*[WSX+20]	98.83%	-/-	0.65/1.69	99.29%	-/-	0.93/1.84
ICP(P2p)[Zha94]	35.57%	0.97/2.08	1.36/8.98	0%	-/2.43	-/160.46
ICP(P2pl)[Zha94]	35.54%	1.00/2.11	1.39/8.99	0%	-/2.44	-/160.45
RANSAC[RBB09b]	33.95%	0.98/2.75	1.37/12.01	15.61%	1.33/4.57	1.79/37.31
FGR[ZPK16]	34.54%	0.98/5972.31	1.2/12.79	17.16%	1.32/35109.13	1.76/28.98
TEASER++[YSC20]	34.06%	0.98/2.72	1.33/15.85	17.13%	1.34/3.83	1.93/29.19
OverlapNet*[CLM+22]	83.86%	-/-	1.28/3.89	0.10%	-/-	2.03/65.45
RPMNet[YL20]	47.31%	1.05/2.07	0.60/1.88	27.80%	1.28/2.42	1.77/13.13
DCP[WS19]	50.71%	0.98/1.83	1.14/6.61	0%	-/4.01	-/161.24
Ours	98.0%	0.85/0.95	0.55/0.70	97.0%	1.00 / 1.15	0.80 /1.00

with temporal probabilistic reasoning, our method achieves substantial improvements in both accuracy and robustness for loop closure detection in autonomous navigation systems.

The core innovation of PNE-SGAN lies in two complementary enhancements to semantic graph-based place recognition. First, we introduced the integration of Normal Distributions Transform (NDT) covariance features as node attributes within the semantic graph framework. Unlike conventional bounding box representations that provide only coarse geometric information, NDT covariance matrices capture the local surface distribution characteristics of semantic objects with higher fidelity. This richer geometric encoding enables the Graph Attention Network to learn more discriminative structural relationships between environmental elements, leading to more distinctive place signatures even in structurally similar environments.

Second, we implemented a comprehensive probabilistic temporal filtering framework that transforms instantaneous graph matching into a principled sequential estimation problem. By modeling loop closure detection as a hidden Markov process, PNE-SGAN explicitly accounts for uncertainties in both odometry measurements and place recognition. The system incorporates graph similarity scores as observation likelihoods within a discrete Bayes filter, while leveraging odometry information with associated uncertainty to construct a coherent motion model based on Mahalanobis distance evaluation. This approach enables robust handling of ambiguous matches through temporal consistency checking, significantly reducing both false positives and false negatives.

A particular strength of our approach is the integration of an "off-map" state within the probabilistic framework, allowing graceful handling of exploration into previously unmapped regions. Furthermore, the implementation of forward-backward smoothing through the application of the forward-backward algorithm provides improved state estimation by incorporating both past and future observations, crucial for reliable loop closure decisions in challenging environments with perceptual aliasing.

Our experimental results demonstrate that PNE-SGAN outperforms state-of-the-art methods across multiple benchmark datasets, achieving higher precision and recall rates while maintaining computational efficiency suitable for real-time operation. The performance improvements are particularly pronounced in challenging scenarios featuring repetitive structures, dynamic objects, and varying sensor viewpoints.

The methodology presented here opens several promising directions for future research. First, exploring alternative geometric descriptors beyond NDT covariance could further enhance discrimination capabilities. Second, investigating online adaptation mechanisms to account for environmental

changes over time would improve long-term autonomy. Finally, integrating PNE-SGAN with hierarchical map representations could enable efficient operation in large-scale environments by reducing the search space for loop closure candidates.

PNE-SGAN represents a significant step toward reliable loop closure detection for LiDAR-based SLAM systems. By addressing the fundamental challenges of geometric representation fidelity and temporal consistency, it provides a robust foundation for autonomous navigation in complex, large-scale environments. The principled uncertainty handling and feature-rich scene representation enable more accurate map corrections, ultimately contributing to improved global consistency in autonomous mapping and localization tasks.

REFERENCES

[BS03] Peter Biber and Wolfgang Straßer. The normal distributions transform: A new approach to laser scan matching. In *Proceedings 2003 IEEE/RSJ International Conference on Intelligent Robots and Systems (IROS 2003)*, volume 3. IEEE, 2003.

[BZ13] Michael Bosse and Robert Zlot. Place recognition using keypoint voting in large 3d lidar datasets. In *2013 IEEE International Conference on Robotics and Automation*, pages 2677–2684. IEEE, 2013.

[CCC+16] Cesar Cadena, Luca Carlone, Henry Carrillo, Yasir Latif, Davide Scaramuzza, José Neira, Ian Reid, and John J Leonard. Past, present, and future of simultaneous localization and mapping: Toward the robust-perception age. *IEEE Transactions on robotics*, 32(6):1309–1332, 2016.

[CLM+21] X. Chen, T. Läbe, A. Milioto, T. Röhling, O. Vysotska, A. Haag, others, and C. Stachniss. Overlapnet: Loop closing for lidar-based slam. *arXiv preprint arXiv:2105.11344*, 2021.

[CLM+22] Xieyuanli Chen, Thomas Läbe, Andres Milioto, Timo Röhling, Jens Behley, and Cyrill Stachniss. Overlapnet: A siamese network for computing lidar scan similarity with applications to loop closing and localization. *Autonomous Robots*, pages 1–21, 2022.

[CMP+19] Xieyuanli Chen, Andres Milioto, Emanuele Palazzolo, Philippe Giguère, Jens Behley, and Cyrill Stachniss. Suma++: Efficient lidar-based semantic slam. In *2019 IEEE/RSJ International Conference on Intelligent Robots and Systems (IROS)*, pages 4530–4537. IEEE, 2019.

[CN08] M. Cummins and P. Newman. Fab-map: Probabilistic localization and mapping in the space of appearance. *The International Journal of Robotics Research*, 27(6):647–665, 2008.

[CVV22] Daniele Cattaneo, Matteo Vaghi, and Abhinav Valada. Lcdnet: Deep loop closure detection and point cloud registration for lidar slam. *IEEE Transactions on Robotics*, 38(4):2074–2093, 2022.

[DCD+18] R. Dubé, A. Cramariuc, D. Dugas, J. Nieto, R. Siegwart, and C. Cadena. Segmap: 3d segment mapping using data-driven descriptors. *arXiv preprint arXiv:1804.09557*, 2018.

[DDS+17] R. Dubé, D. Dugas, E. Stumm, J. Nieto, R. Siegwart, and C. Cadena. Segmatch: Segment based place recognition in 3d point clouds. In *2017 IEEE International Conference on Robotics and Automation (ICRA)*, pages 5266–5272. IEEE, 2017.

[DGS+18] R. Dubé, M. G. Gollub, H. Sommer, I. Gilitschenski, R. Siegwart, C. Cadena, and J. Nieto. Incremental-segment-based localization in 3-d point clouds. *IEEE Robotics and Automation Letters*, 3(3):1832–1839, 2018.

[GLT12] Dorian Gálvez-López and Juan D. Tardos. Bags of binary words for fast place recognition in image sequences. *IEEE Transactions on Robotics*, 28(5):1188–1197, 2012.

[GLU12] Andreas Geiger, Philip Lenz, and Raquel Urtasun. Are we ready for autonomous driving? the kitti vision benchmark suite. In *2012 IEEE Conference on Computer Vision and Pattern Recognition*, pages 3354–3361. IEEE, 2012.

[HWZ16] Li He, Xiaolong Wang, and Hong Zhang. M2dp: A novel 3d point cloud descriptor and its application in loop closure detection. In *2016 IEEE/RSJ International Conference on Intelligent Robots and Systems (IROS)*. IEEE, 2016.

[JS23] Binqian Jiang and Shaojie Shen. Contour context: Abstract structural distribution for 3d lidar loop detection and metric pose estimation. In *2023 IEEE International Conference on Robotics and Automation (ICRA)*. IEEE, 2023.

[K+20] Xin Kong et al. Semantic graph based place recognition for 3d point clouds. In *2020 IEEE/RSJ International Conference on Intelligent Robots and Systems (IROS)*. IEEE, 2020.

[KCK21a] Giseop Kim, Sunwook Choi, and Ayoung Kim. Scan context++: Structural place recognition robust to rotation and lateral variations in urban environments. *IEEE Transactions on Robotics*, 38(3):1856–1874, 2021.

[KCK21b] Giseop Kim, Sunwook Choi, and Ayoung Kim. Scan context++: Structural place recognition robust to rotation and lateral variations in urban environments. *IEEE Transactions on Robotics*, 38(3):1856–1874, 2021.

[KK18] Giseop Kim and Ayoung Kim. Scan context: Egocentric spatial descriptor for place recognition within 3d point cloud map. In *2018 IEEE/RSJ International Conference on Intelligent Robots and Systems (IROS)*. IEEE, 2018.

[LKZ+21] Lin Li, Xin Kong, Xiangrui Zhao, Teng Huang, Wanlong Li, Feng Wen, Hongbo Zhang, and Yong Liu. Ssc: Semantic scan context for large-scale place recognition. In *2021 IEEE/RSJ International Conference on Intelligent Robots and Systems (IROS)*, pages 5080–5085. IEEE, 2021.

[LM13] Mathieu Labbe and François Michaud. Appearance-based loop closure detection for online large-scale and long-term operation. *IEEE Transactions on Robotics*, 29(3):734–745, 2013.

[LM19] M. Labbé and F. Michaud. Rtab-map as an open-source lidar and visual simultaneous localization and mapping library for large-scale and long-term online operation. *Journal of Field Robotics*, 36(2):416–446, 2019.

[M+22] Junyi Ma et al. Overlaptransformer: An efficient and yaw-angle-invariant transformer network for lidar-based place recognition. *IEEE Robotics and Automation Letters*, 7(3):6958–6965, 2022.

[MAT17] R. Mur-Artal and J. D. Tardós. Orb-slam2: An open-source slam system for monocular, stereo, and rgb-d cameras. *IEEE Transactions on Robotics*, 33(5):1255–1262, 2017.

[MLD17] Martin Magnusson, Achim J Lilienthal, and Tom Duckett. Semi-supervised 3d place categorisation by descriptor clustering. In *2017 IEEE/RSJ International Conference on Intelligent Robots and Systems (IROS)*, pages 3616–3623. IEEE, 2017.

[MMW12] W. Maddern, M. Milford, and G. Wyeth. CAT-SLAM: probabilistic localisation and mapping using a continuous appearance-based trajectory. *The International Journal of Robotics Research*, 31(4):429–451, 2012.

[MMW13] Will Maddern, Michael Milford, and Gordon Wyeth. Towards persistent localization and mapping with a continuous appearance-based topology. In *Robotics: Science and Systems VIII*, page 281, 2013.

[QSMG17] Charles R Qi, Hao Su, Kaichun Mo, and Leonidas J Guibas. Pointnet: Deep learning on point sets for 3d classification and segmentation. In *Proceedings of the IEEE Conference on Computer Vision and Pattern Recognition*, pages 652–660, 2017.

[Rab89] Lawrence R. Rabiner. A tutorial on hidden Markov models and selected applications in speech recognition. *Proceedings of the IEEE*, 77(2):257–286, 1989.

[RBB09a] Radu Bogdan Rusu, Nico Blodow, and Michael Beetz. Fast point feature histograms (fpfh) for 3d registration. In *2009 IEEE International Conference on Robotics and Automation*, pages 3212–3217. IEEE, 2009.

[RBB09b] Radu Bogdan Rusu, Nico Blodow, and Michael Beetz. Fast point feature histograms (fpfh) for 3d registration. In *2009 IEEE International Conference on Robotics and Automation*, pages 3212–3217. IEEE, 2009.

[SEG15] Thomas Schmiedel, Erik Einhorn, and Horst-Michael Gross. Iron: A fast interest point descriptor for robust ndt-map matching and its application to robot localization. In *2015 IEEE/RSJ International Conference on Intelligent Robots and Systems (IROS)*, pages 3190–3197. IEEE, 2015.

[SM24] Matteo Scucchia and Davide Maltoni. Region prediction for efficient robot localization on large maps. In *International Conference on Robotics, Computer Vision and Intelligent Systems*, Cham, 2024. Springer Nature Switzerland.

[SML12] T. Stoyanov, M. Magnusson, and A. J. Lilienthal. Point set registration through minimization of the l 2 distance between 3d-ndt models. In *2012 IEEE International Conference on Robotics and Automation*, pages 5196–5201. IEEE, 2012.

[STDS14] Samuele Salti, Federico Tombari, and Luigi Di Stefano. Shot: Unique signatures of histograms for surface and texture description. *Computer Vision and Image Understanding*, 125:251–264, 2014.

[UL18] Mikaela Angelina Uy and Gim Hee Lee. Pointnetvlad: Deep point cloud based retrieval for large-scale place recognition. In *Proceedings of the IEEE Conference on Computer Vision and Pattern Recognition*. IEEE, 2018.

[VCC+17] P. Velickovic, G. Cucurull, A. Casanova, A. Romero, P. Lio, and Y. Bengio. Graph attention networks. *stat*, 1050(20):10–48550, 2017.

[VMH+21] K. Vidanapathirana, P. Moghadam, B. Harwood, M. Zhao, S. Sridharan, and C. Fookes. Locus: Lidar-based place recognition using spatiotemporal higher-order pooling. In *2021 IEEE International Conference on Robotics and Automation (ICRA)*, pages 5075–5081. IEEE, 2021.

[VSP+17] Ashish Vaswani, Noam Shazeer, Niki Parmar, Jakob Uszkoreit, Llion Jones, Aidan N. Gomez, Lukasz Kaiser, and Illia Polosukhin. Attention is all you need. *Advances in Neural Information Processing Systems*, 30, 2017.

[WS19] Yue Wang and Justin M. Solomon. Deep closest point: Learning representations for point cloud registration. In *Proceedings of the IEEE/CVF International Conference on Computer Vision*, pages 3523–3532, 2019.

[WSX+20] Y. Wang, Z. Sun, C. Z. Xu, S. E. Sarma, J. Yang, and H. Kong. Lidar iris for loop-closure detection. In *2020 IEEE/RSJ International Conference on Intelligent Robots and Systems (IROS)*, pages 5769–5775. IEEE, 2020.

[WWX20] Han Wang, Chen Wang, and Lihua Xie. Intensity scan context: Coding intensity and geometry relations for loop closure detection. In *2020 IEEE International Conference on Robotics and Automation (ICRA)*. IEEE, 2020.

[X+21] Ming Xu et al. Probabilistic appearance-invariant topometric localization with new place awareness. *IEEE Robotics and Automation Letters*, 6(4):6985–6992, 2021.

[XXW+21] Yan Xia, Yusheng Xu, Shuang Wang, Mingze Yan, Shangshu Kang, and Xuezhi Tang. Soe-net: A self-attention and orientation encoding network for point cloud based place recognition. In *Proceedings of the IEEE/CVF Conference on Computer Vision and Pattern Recognition*, pages 11348–11357, 2021.

[XYC+21] X. Xu, H. Yin, Z. Chen, Y. Li, Y. Wang, and R. Xiong. Disco: Differentiable scan context with orientation. *IEEE Robotics and Automation Letters*, 6(2):2791–2798, 2021.

[YL20] Zi Jian Yew and Gim Hee Lee. Rpm-net: Robust point matching using learned features. In *Proceedings of the IEEE/CVF Conference on Computer Vision and Pattern Recognition*, pages 11824–11833, 2020.

[YMA+25] L. Yang, R. Mascaro, I. Alzugaray, S. M. Prakhya, M. Karrer, Z. Liu, and M. Chli. Lidar loop closure detection using semantic graphs with graph attention networks. *Journal of Intelligent & Robotic Systems*, 111(1):1–16, 2025.

[YSC20] Hao Yang, Jingming Shi, and Luca Carlone. Teaser: Fast and certifiable point cloud registration. *IEEE Transactions on Robotics*, 37(2):314–333, 2020.

[Z+21] Zhicheng Zhou et al. Ndt-transformer: Large-scale 3d point cloud localisation using the normal distribution transform representation. In *2021 IEEE International Conference on Robotics and Automation (ICRA)*. IEEE, 2021.

[Zha94] Zhengyou Zhang. Iterative point matching for registration of free-form curves and surfaces. *International Journal of Computer Vision*, 13(2):119–152, 1994.

[ZPK16] Qian-Yi Zhou, Jaesik Park, and Vladlen Koltun. Fast global registration. In *Computer Vision–ECCV 2016: 14th European Conference, Amsterdam, The Netherlands, October 11-14, 2016, Proceedings, Part II*, volume 14. Springer International Publishing, 2016.

[ZWP+22] Youjie Zhou, Yiming Wang, Fabio Poiesi, Qi Qin, and Yi Wan. Loop closure detection using local 3d deep descriptors. *IEEE Robotics and Automation Letters*, 7(3):6335–6342, 2022.

[ZX19] Wenxiao Zhang and Chunxia Xiao. Pcan: 3d attention map learning using contextual information for point cloud based retrieval. In *Proceedings of the IEEE/CVF Conference on Computer Vision and Pattern Recognition*, pages 7373–7382, 2019.